TOPICAL REVIEW • OPEN ACCESS

Covalent polymer functionalization of graphene/graphene oxide and its application as anticorrosion materials

To cite this article: Ihsan Amin *et al* 2022 *2D Mater.* **9** 032002

2D Materials

OPEN ACCESS

RECEIVED
7 August 2021

REVISED
18 January 2022

ACCEPTED FOR PUBLICATION
14 February 2022

PUBLISHED
10 June 2022

TOPICAL REVIEW

Covalent polymer functionalization of graphene/graphene oxide and its application as anticorrosion materials

Ihsan Amin[1], **Erdni Batyrev**[2], **Arnoud de Vooys**[2], **Hans van der Weijde**[2] **and N Raveendran Shiju**[1,*]

[1] Van't Hoff Institute for Molecular Sciences, University of Amsterdam, Science Park 904, 1098 XH Amsterdam, The Netherlands
[2] Tata Steel Research and Development, PO Box 10.000, 1970CA IJmuiden, The Netherlands
* Author to whom any correspondence should be addressed.

E-mail: n.r.shiju@uva.nl

Keywords: graphene, coatings, anti-corrosion, polymers, steel

Abstract

Research on grapheme-polymer composites as the promising ion barrier materials to tackle the corrosion issue is rapidly developing and attracts interests from both academia and industry. In this minireview, we highlight the covalent functionalization of graphene and its derivatives such as graphene oxide (GO) with polymer brushes, and their application in anticorrosion within the last 3 years. There are some recent excellent reviews published on single layer graphene and graphene-based polymer composites for anticorrosion. However, the covalent functionalization of graphene and GO with polymer brushes for application in anticorrosion has not been addressed in those reviews. In this review, we describe first the current state of the art of covalent functionalization of graphene/GO with polymer brushes. We then discuss the application of pristine graphene as anticorrosion material and its drawbacks which can be overcome by graphene-based polymer composites. Afterwards, we discuss in detail the recent progress and development of covalent polymer functionalized graphene/GO as anticorrosion coatings, reported within the last 3 years. Finally, as perspective, we will briefly summarize the work on composites of polymers with other two-dimensional (2D) materials as anticorrosion coatings. Herein, hexagonal boron nitride, the most studied 2D materials after graphene, and $Ti_3C_2T_x$ MXene which is the rising star of 2D transition metal carbide/nitride will be discussed.

1. Introduction

Corrosion, a tendency of metal to convert to its oxide form, has a significant environmental and economic impact in society. It also poses a significant safety issue in several aspects of our society spanning from industrial plants to buildings and bridges. The annual cost of corrosion is US$ 2.2 trillion or 3% of world's GDP, whereas in US–UK–China alone, it costs 5% of the annual GDP [1]. This data is for corrosion of steel only and the annual cost will be much higher if we consider also other metals. To prevent the corrosion, anti-corrosive coatings are used and hexavalent chromium (Cr^{VI+}) has become a golden standard for such anticorrosion coatings [2, 3]. However, Cr (VI) is toxic, and carcinogenic [4, 5]. Therefore, it is necessary to find another alternative which is environmentally friendly, safe and offers long term durability. In this respect, graphene and its derivatives have emerged as alternative components for anticorrosion coating which can meet the above requirements [6, 7].

Graphene is undoubtedly the most well studied two-dimensional (2D) material in the last decade [8]. Owing to its superior intrinsic optical [9], electrical [10], and mechanical properties [11], graphene has been used for the applications in energy harvesting [12, 13] and storage [14, 15], catalysis [16–18], as well as for applications such as biosensors [19–21]. There were also significant efforts by academia and industries for the incorporation of graphene and graphene-based composites in flexible electronics and wearable technologies [22]. Therefore, several reviews were dedicated for graphene and graphene-based composites and their applications in the above mentioned applications.

One of the interesting properties of graphene is its super impermeability, even to smallest gas atom such as helium [23]. This property has made graphene and graphene-based composites as suitable

candidates for safe and environmentally friendly anticorrosion coatings. As the impermeability property of graphene is rather overlooked and less investigated compared to the optical, electrical and mechanical properties and their application thereof, the reviews discussing the application of graphene and graphene-based composites for anticorrosion are relatively limited.

The surface functionalization of graphene has become a popular technique to make it more suitable for various applications. Both noncovalent and covalent functionalization of graphene were investigated for this purpose [24]. The covalent functionalization of graphene is preferred for long term performance and stability [25]. Therefore, this is the most favourable route to prepare graphene-based polymeric composites [24, 25]. Polymer brushes are chains of polymers with one end grafted to a surface [26, 27]. The physicochemical properties of the polymer brushes can be tuned to meet the desired applications [28, 29]. Moreover, the grapheme-polymer composite systems offer versatility and advantage for further functionalization such as the incorporation with metal nanoparticles [30]. This opens even more applications including the anticorrosion coatings.

There are a few recent excellent reviews on graphene-based composites for anticorrosion [31–35]. However, the covalent functionalization of graphene and graphene oxide (GO) with polymeric materials is not discussed in them. Given the importance of the functionalization approach in achieving long term stability of the composites, in this minireview, we will specifically discuss this topic, and their application in anticorrosion in last 3 years.

2. Covalent functionalization of graphene with polymeric materials

Surface covalent functionalization of graphene with polymeric materials has become the most interesting functionalization route as it offers several advantages. Firstly, the combination of the properties of graphene and the functional polymeric materials may result in synergy and an enhancement of the properties of the synthesized composites. Secondly, post-functionalization of the polymeric materials is possible to introduce broader range of functionalities such as impregnation with nanoparticles or bioconjugation. Finally, covalent functionalization may guarantee the long-term stability of the composites. Hereafter, we discuss a couple of covalent functionalization methods, namely, (a) self-initiated photografting and photopolymerization (SIPGP) and (b) dopamine (DA)-mediated surface-initiated atom transfer radical polymerization (SI-ATRP). Both are simple with low-cost experimental procedure that requires no sophisticated laboratory equipment. Owing to their simplicity, both methods can be easily scaled-up which is necessary for commercial application and therefore, can be easily adopted by the researchers in academia and industries working in anticorrosion field to prepare graphene-based polymer composite coatings.

2.1. Self-initiated photografting and photopolymerization (SIPGP)

The covalent functionalization of graphene, mediated by diazonium salt usually results in an increase of the defect sites on the graphene itself [36, 37], which may degrade the functionality of the composites. Therefore, developing new methods for covalent functionalization of graphene without increasing the defect sites is required. UV-induced photopolymerization, commonly refers as SIPGP [38–41] has emerged as a powerful method which addresses this requirement. Steenackers *et al* [42] has prepared patterned polystyrene (PS) brushes on graphene monolayers by combining SIPGP and photolithography. In their work, a quantifoil TEM mask with opening of 40 μm was placed on the top of chemical vapour deposition (CVD) grown monolayer graphene on copper. Subsequently, the substrate was submerged in predegassed bulk styrene monomer in a glass tube. Next, the polymerization was performed by irradiation of the system with UV light (λ_{max} = 350 nm, power density of ~5 mW cm^{-2}) for 16 h, resulting in 10 nm thick PS layer. Graphene bears native sp^3 hybridized defects. The hydrogen from these defect sites can be abstracted upon UV irradiation which generate local radicals that initiate the free radical polymerization of styrene. Previous studies showed that basal plane conjugation of the graphene is not distorted by UV irradiation and hence there is no degradation of its electronic properties. Even though it is not completely clear why UV polymerization method does not create additional defects, it is most likely due to the fact that the polymerization occurs on the already-existing defect sites. As the PS brushes stabilize the system, the patterned PS brushes on graphene can be entirely lifted of by etching the copper layer using ammonium persulfate (APS). This results in a freestanding graphene-based polymer carpet which can be transferred to any substrates, including onto the silicon wafer for further surface characterization.

The successful covalent functionalization of the PS brushes on the graphene layer was proved by Infrared and Raman spectroscopy (figures 1(a)–(c)). As shown in figure 1(a), the characteristic vibrational modes of PS are observed on the covalently grafted PS brushes on graphene, that include the aromatic group, (ν_{C-H} at ~3024 cm^{-1} and ν_{C-C} between 1454 and 1601 cm^{-1}) and the methylene groups of the polymer backbone (ν_{C-H} ~ 2919 cm^{-1}). Figure 1(b) shows the comparison of the Raman spectra from bulk PS and graphene. While the observed modes are well separated in the region near the 2D graphene band, there is significant spectral overlap in the region of the D and G bands. Therefore, for quantitative analysis

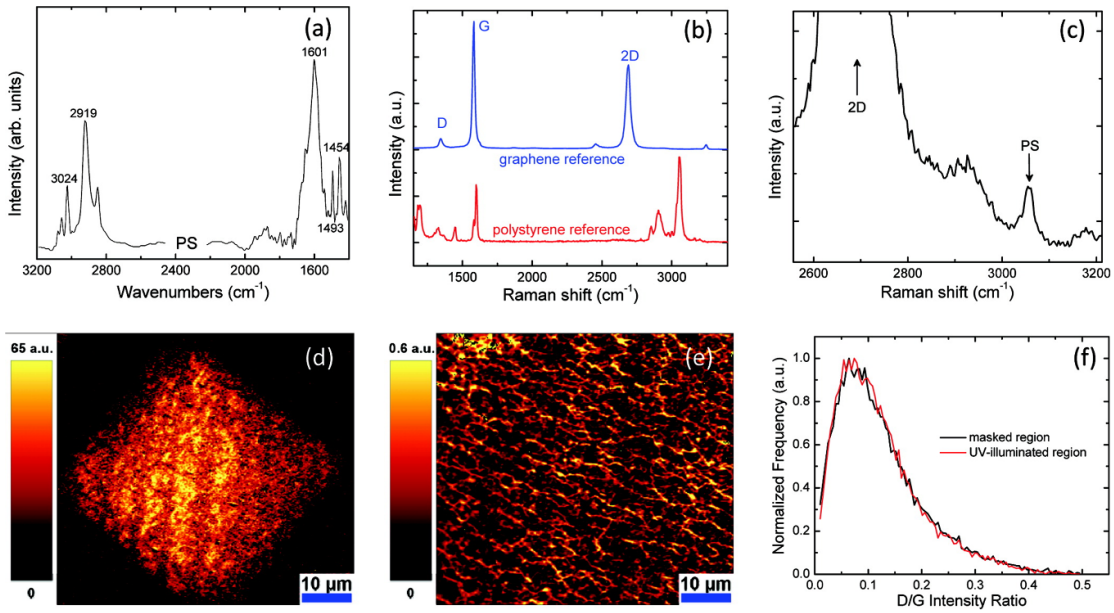

Figure 1. (a) IR spectra of the patterned PS brushes on graphene transferred on silicon wafer. (b) Comparison of Raman spectra of monolayer graphene transferred on silicon wafer and bulk PS. (c) The intensity of Raman spectrum of primary PS brush peak as obtained by SIPGP is ∼40× smaller than that of graphene 2D mode. (d) Raman mapping of the integrated intensity from PS in the range of 3000–3100 cm^{-1}. (f) The D/G intensity of the same region in (d). (g) The histogram of the D/G intensity ratio in PS brush area and graphene-only area shows no change in the intensity ratio. Figures (a)–(g): Reprinted with permission from [42]. © 2011, American Chemical Society.

of the D and G mode intensities, the appropriate PS contribution to the total scattering intensity was subtracted from each region of interest based on reference data and the PS intensity at the maximum near 3055 cm^{-1}. Figure 1(c) shows the Raman spectrum near the 2D mode obtained in an illuminated region which contains contributions from both PS and graphene. Though the total contribution from PS is small, the signal is readily resolved. Raman mapping was conducted to compare the patterned area and graphene-only area, as well as the D/G mode intensity of the same region, as shown in figures 1(d) and (e), respectively. The histogram of the D/G intensity ratio in PS brush area and graphene-only area are comparable and shows no change in the intensity ratio (figure 1(f)). This indicates that the UV-photopolymerization does not generate additional defects and the grafting occurs preferentially on the existing edge defect sites.

In another work, Seifert *et al* [43] demonstrated the preparation of functional block copolymer brushes on the hydrogenated graphene via consecutive SIPGP. In the 1st step, styrene was directly grafted on the hydrogenated graphene. In the 2nd step, copolymerisation of styrenes and acrylates and consecutive SIPGP of both monomer types were used to make functional polymer brushes of poly(styrene-co-acrylate). This consecutive SIPGP method not only proves the livingness of the polymer chains grown by SIPGP, but also can be easily adopted to prepare graphene-based block copolymers for anticorrosion coatings.

In another approach, the UV photopolymerization was combined with Kumada catalyst transfer photocondensation (KCTP) technique to grow the conductive poly(3-hexylthiophene) P3HT brushes on monolayer graphene, as shown in figure 2(a) [44]. Figure 2(a) shows the mechanism of the growth of conductive P3HT brushes on graphene. Since graphene bears native sp^3 hybridized defects, the hydrogen from these defect sites can be abstracted upon UV irradiation, generating local radicals that initiate the free radical polymerization of 4-bromostyrene. The covalently attached aryl bromide of PSBr on graphene undergoes an oxidative addition by placing it in a solution of $Ni(PPh_3)_4$. The reaction is followed by the ligand exchange with the 1,3-bis(diphenylphosphino)propane (dppp), resulting in a surface-bound, metal-mediated coupling catalyst. The dppp leads to the highest degree of the polymerization control in the P3HT synthesis in solution. Surface initiated (SI)-KCTP was initiated by the addition of 2-bromo-5-chloromagnesio-3-hexylthiophene dissolved in tetrahydrofuran [44]. Afterwards, a thin layer of P3HT brush layer covering the entire graphene interface was observed. The graphene-based conductive polymer carpets showed potential application for flexible optoelectronics. As both graphene and conductive polymers [45, 46] are promising materials for anticorrosion, the graphene-based P3HT carpets may exhibit synergistic or enhanced anticorrosion properties. Sheng *et al* synthesized functionalized graphene/-polyaniline composites which demonstrated

effective synergistic reinforcement on anticorrosion [47].

2.2. DA-mediated SI-ATRP

Another emerging strategy to achieve covalent functionalized polymer brushes on graphene materials is to combine mussel-inspired DA interfacial chemistry and SI-ATRP. The SI-ATRP has become a gold standard for surface functionalization with polymer brushes having broad range of functionalities [48]. However, this method is limited only to gold, silicon or metal oxide substrates as the utilization of self-assembled monolayers and subsequent attachment with appropriate initiator are necessary. Therefore, direct SI-ATRP on graphene materials was not really attempted. Nevertheless, there are ways to overcome this. Since the seminal paper by Messersmith *et al* [49] polydopamine (PDA) has been emerged as a universal and efficient medium for surface functionalization or as interfacial layer. PDA can adhere onto various surfaces, including polymers, metals, and ceramics [50–52]. Owing to the abundant amine and hydroxyl functional groups in DA, subsequent chemical functionalization of the PDA interfacial layer with polymer brushes are realizable. Moreover, it has been proven that DA can act as green and cheap reducing agent for GO [53]. Luo *et al* [54] reported an innovative and universal method for the fabrication of covalent functionalized graphene-polymer composites by combining the PDA chemistry and SI-ATRP as shown in figure 3. First, they prepared macroinitiator bearing DA and bromo isobutyrate bromide (BIBB) initiator layer (DA-BIBB). Next, graphene sheets were coated with DA-BIBB to obtain rGO@PDA-Br. Subsequentially, PS brushes were grown. The process is shown schematically in figures 3(a)–(c). Besides XPS, UV–Vis and FTIR spectroscopy, they used Raman spectroscopy to verify the success of each step of functionalization. Figure 3(d) shows the Raman spectra of GO, rGO@PDA-Br, and rGO@PDA-PS, respectively. GO shows the expected D band and G band at 1348 cm^{-1} and 1598 cm^{-1}, respectively. For rGO@PDA-Br, D band is at 1337 cm^{-1} and G band is at 1588 cm^{-1}. This red-shift of about 10 cm^{-1} clearly indicates high degree of the reduction. Interestingly, after SI-ATRP of growing PS brushes, the position of D and G bands of rGO@PDA-PS are 1336.9 cm^{-1} and 1587.6 cm^{-1}, respectively, similar to those from rGO@PDA-Br.

Furthermore, their calculation shows that the value of intensity ratio I_D/I_G are increasing from 0.87 for GO, 0.93 for rGO@PDA-Br, and 1.09 for rGO@PDA-PS. While in general, an increase in the value of the I_D/I_G ratio indicates the introduction of defect on graphene, another important aspect to look at is the negligible changes in the position of D and G bands for rGO@PDA-Br and rGO@PDA-PS. This indicates that the covalent grafting of PS brush chains is preferentially on the initiator part, not on graphene itself. This conclusion fits well with their assertion that combining the mussel-inspired DA chemistry and SI-ATRP for preparation of PS brushes on graphene materials is a bridge between noncovalent methods from GO to rGO@PDA-Br, followed by the covalent functionalization of the latter with PS brushes to achieve rGO@PDA-PS composites. In similar fashion, recently, Wang *et al* [55] demonstrated the covalent grafting of poly(glycidyl methacrylate) (PGMA) and poly(N,N, dimethylaminoethyl methacrylate) (PDMAEMA) brushes on graphene sheets using PDA interface layer. PDMAEMA is pH and thermoresponsive polymer which exhibits not only antifouling properties but also corrosion resistance [56]. Cui *et al* [57] reported that PDA-grafted graphene showed a remarkable improvement in the corrosion protection performance of waterborne epoxy coatings (WECs). Later on, Qian *et al* [58] demonstrated that PDA-based coated-nanocontainer shows self-healing properties to repair defects and prevent further corrosion. These self-healing behaviour and protection properties can be modulated by pH owing to PDA sensitivity to pH. Similar work was reported by Chen *et al* [59] where they utilized the self-healing behaviour of PDA-coated halloysite nanotubes self-assembled on GO for enhancing corrosion resistance of WEC. We envisage that the combined covalent functionalization of PDA and polymer brushes on graphene materials will exhibit synergistic effect which may further improve corrosion resistance.

3. Anticorrosion performance of graphene and graphene-polymer brush composites

3.1. Anti-corrosion properties of pristine CVD graphene

In the early stage of research, it was found that the single-layer CVD graphene (SL-graphene) exhibits anticorrosive properties. Chen *et al* [6] showed that the SL-graphene inhibits the corrosion on Cu and Cu/Ni alloy. Figure 4 shows SEM and XPS measurements of metal surfaces before and after air oxidation. The atomic steps under the graphene film are clearly visible for graphene-coated samples before and after annealing (figures 4(a)–(c); top), indicating that copper oxide has not formed beneath the graphene. As shown by XPS, the graphene coated Cu and Cu/Ni surfaces are free from surface oxide due to the H_2(g) exposure at a high temperature (1000 °C) prior to the growth of graphene. The metal surface is protected by the graphene layer during subsequent extended exposure at 200 °C in air.

The XPS spectra of graphene-coated Cu foil before and after air annealing (200 °C, 4 h) show two Cu peaks at binding energies of 932.6 eV and 952.5 eV, corresponding to $Cu2p_{3/2}$ and $Cu2p_{1/2}$ (figure 4(b)). Whereas, the uncoated Cu foil shows broader peaks which correspond to different copper

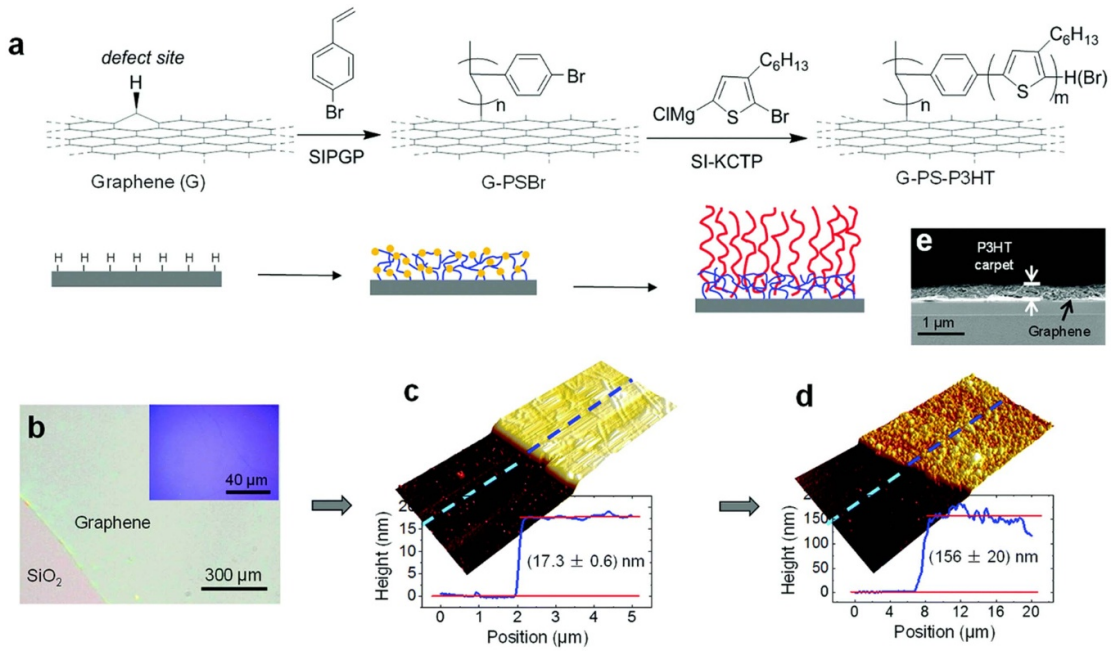

Figure 2. Graphene-based conductive polymer carpets. (a) Schematic illustration of the conductive polymer carpets by the combination of UV-photopolymerization and KCTP. (b) Optical microscope image of monolayer graphene on silicon wafer. AFM height image and its corresponding height profile. (c) After UV-photopolymerization of PS–Br brushes on graphene. (d) After subsequent growth of conductive P3HT brushes. Reproduced by permission of The Royal Society of Chemistry, from [44]. Copyright 2018 the Royal Society of Chemistry.

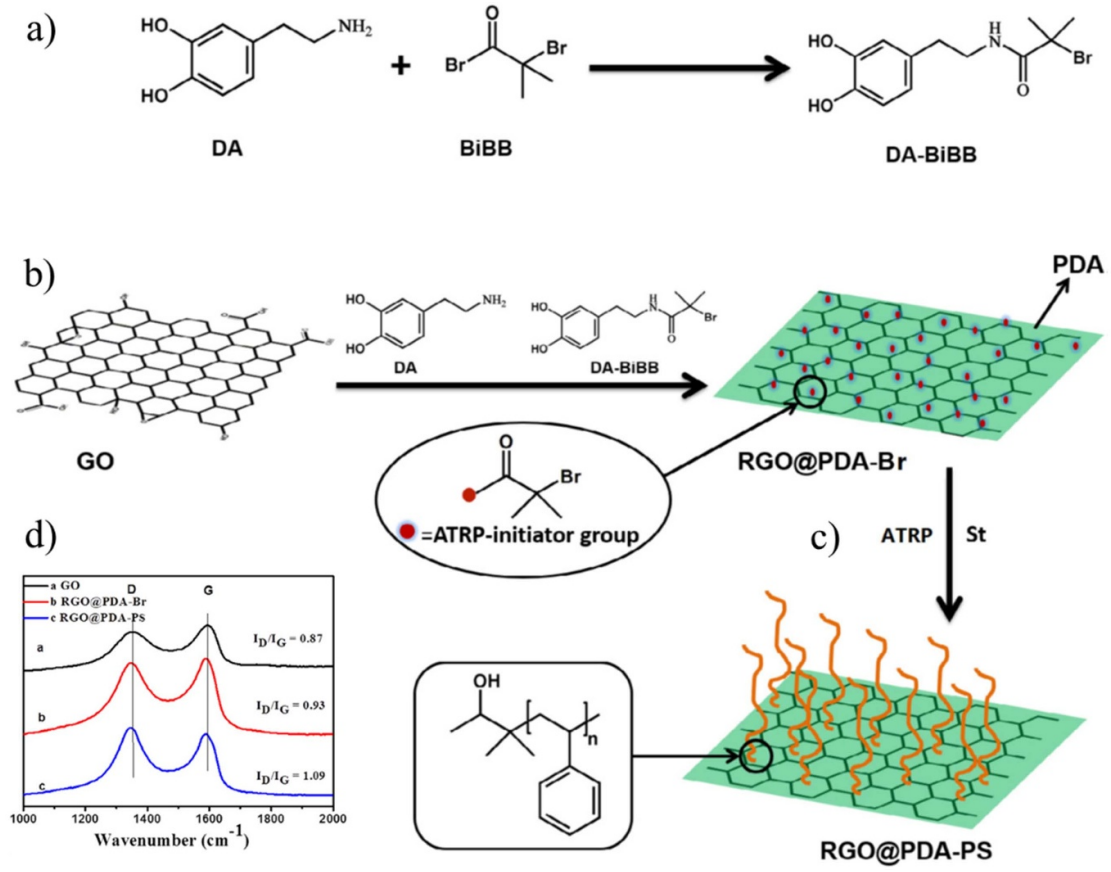

Figure 3. Schematic illustration of the fabrication of covalent functionalized graphene-based polymer composites by combining mussel-inspired DA and SI-ATRP. (a) Preparation of DA-BIBB macro initiator; (b) functionalization of GO with DA-BIBB leading to rGO@PDA-Br; (c) SI-ATRP to grow PS brushes, rGO@PDA-PS; (d) Raman spectra of GO, rGO@PDA-Br and rGO@PDA-PS. Figures (a)–(d): Reprinted from [54], © 2016 Elsevier B.V. All rights reserved.

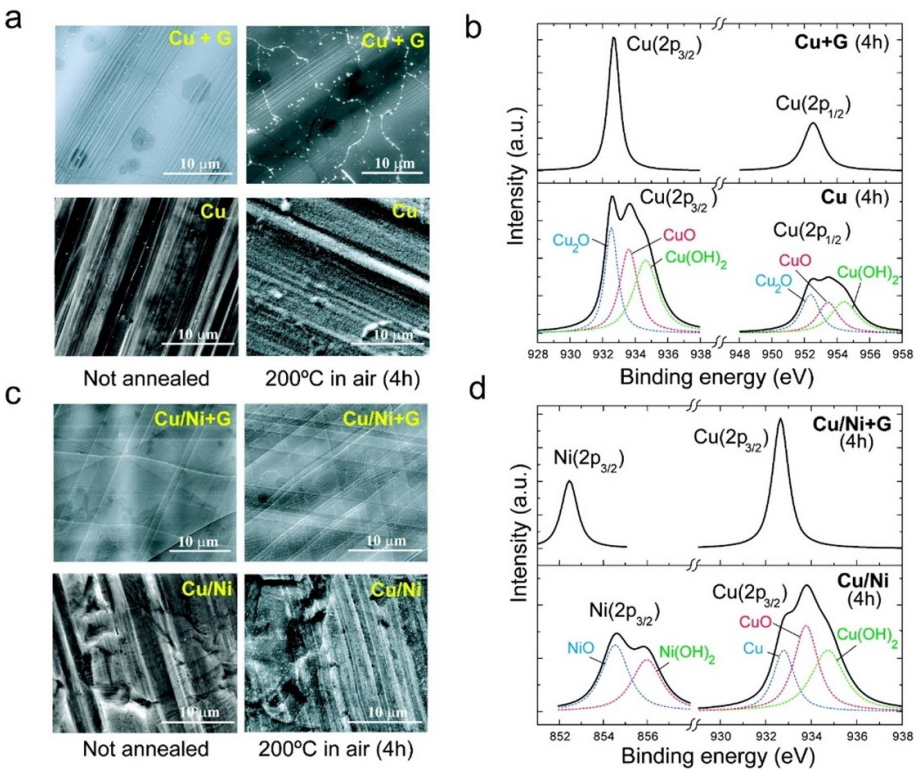

Figure 4. (a) SEM images of graphene coated (upper) and uncoated (lower) Cu foil taken before (left column) and after (right column) annealing in air. (b) XPS core-level Cu2p spectrum of coated (upper) and uncoated (lower) Cu foil after air anneal (200 °C, 4 h). (c) SEM images of graphene coated (upper) and uncoated (lower) Cu/Ni foil taken before (left column) and after (right column) annealing in air. (d) XPS core-level $Ni2p_{3/2}$ and $Cu2p_{3/2}$ spectra of coated (upper) and uncoated (lower) Cu/Ni foils after air annealing (200 °C, 4 h). Figures (a)–(d): Reprinted with permission from [6]. © 2011, American Chemical Society.

oxides, Cu_2O (932.5 eV and 952.3 eV), CuO (933.6 eV and 953.4 eV), and $Cu(OH)_2$ (934.7 eV and 954.5 eV). Similarly, figure 4(d) shows the XPS spectrum for the coated Cu/Ni foil. The binding energy values of the two sharp peaks, corresponding to $Cu2p_{3/2}$ (932.6 eV) and $Ni2p_{3/2}$ (852.5 eV), indicate no change in the chemical composition of the protected metal. As before, inspection of the uncoated foil reveals two broader peaks, one is composed of two nickel oxide peaks, NiO (854.5 eV) and $Ni(OH)_2$ (856.0 eV), and the other is composed of three peaks—metallic Cu (932.6 eV) and two copper oxide peaks, CuO (933.6 eV), and $Cu(OH)_2$ (934.7 eV). These XPS spectra demonstrate that the uncoated Cu/Ni foil was oxidized to a certain extent after heat treatment. The data in figure 4(d) also provide a means to compare graphene as a protection layer with the inherent corrosion resistance of Cu/Ni alloy. Upon oxidation, the uncoated Cu/Ni alloy forms a protective film of Cu_2O with Ni compounds (e.g. NiO) as minor components. This oxide layer is more stable due to the presence of Ni atoms in the copper lattice, resulting in a lower number of defects. The oxide prevents further oxidation, which explains the presence of a metallic Cu signal in figure 4(d) (lower). Nevertheless, the graphene-coated Cu/Ni alloy still shows significantly better oxidation resistance, compared to the uncoated Cu/Ni alloy, as can be seen from the absence of oxide signals in figure 4(d) (upper).

These data indicate that the graphene coating is clearly acting as a diffusion barrier, protecting the underlying Cu and Cu/Ni from oxidation. Prasai *et al* [7] also reported that SL-graphene protects and inhibits corrosion on Cu and Ni metals in aerated Na_2SO_4 solution. Zhou *et al* [60] grew SL-graphene on stainless steel (G/steel) and compared its anti-corrosion properties with pristine stainless steel, as shown in figure 5.

The corrosion rate of pristine stainless steel was 1.75×10^{-13} ms^{-1} and for the graphene-coated stainless steel was only 2.02×10^{-14} ms^{-1} (figure 5(b)). Even after immersing in a 5% NaCl solution for 30 d, graphene-coated stainless steel still showed low corrosion rate (figure 5(d)). While pristine stainless steel was corroded severely (figure 5(e)), the graphene-coated stainless steel showed no significant changes (figure 5(f)). However, later studies showed that SL-graphene is not suitable for long-term corrosion protection, since wrinkles and defects developed on SL-graphene may act as permeation sites for the ions and even monomers [61]. Schriver *et al* [62] reported that there was severe galvanic corrosion for graphene on Cu at ambient conditions on long-term. Later studies found that

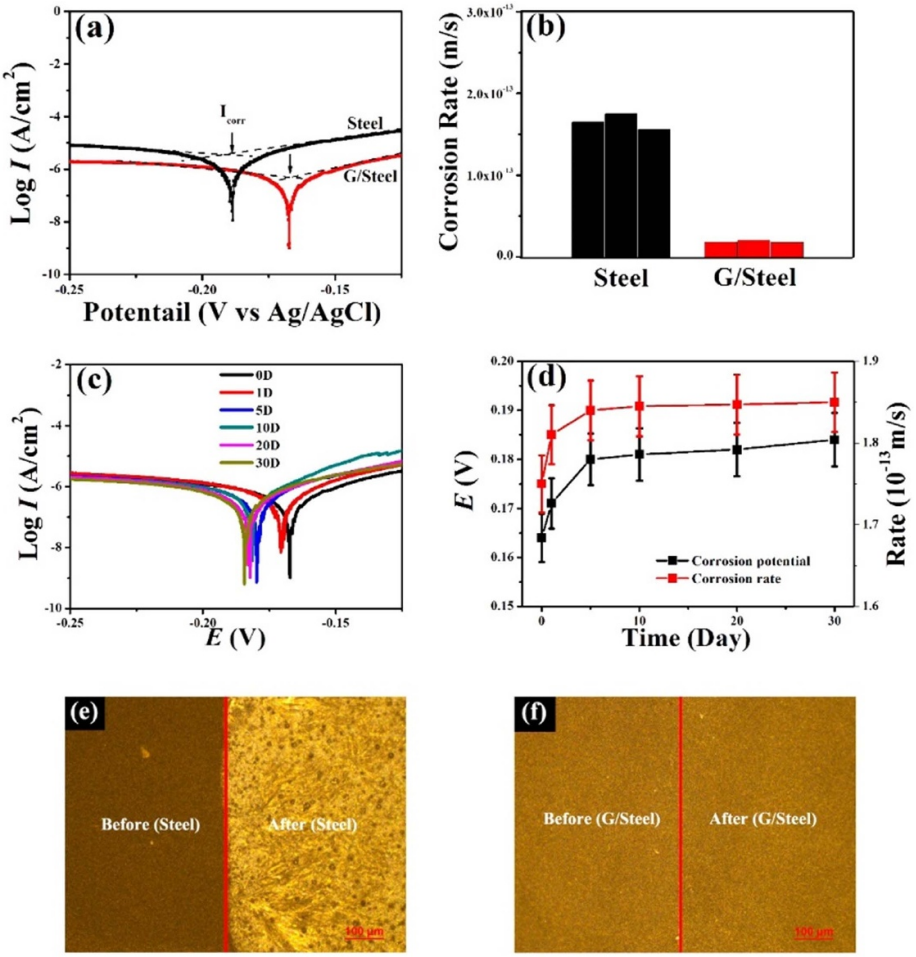

Figure 5. (a) Tafel plots of steel and G/steel substrates after immersion in 5% NaCl solution. (b) The corrosion rates of stainless steel and G/steel samples as calculated from Tafel plots. (c) The current–voltage curve vs time. (d) The corrosion potentials and corrosion rate as a function of the time in the G/steel sample. Optical images of (e) pristine stainless steel and (f) G/steel substrate before and after electrochemical anticorrosion experiment. Figures (a)–(f): Reprinted with permission from [60]. © 2016, American Chemical Society.

corrosion occurred on the defect sites acts similarly to a cathode that accelerates corrosion [63]. As schematically illustrated in figure 6, the defect areas provide permeation pathways and accelerate metal corrosion due to micro-galvanic corrosion, thus, disrupting the corrosion protection [64, 65].

To overcome this problem, many researchers reported several ways to achieve long term corrosion protection with graphene-based coatings. Weatherup *et al* [66] have reported that forming locally passivating oxide close to damage regions or defect sites, plugging the defects to prevent the oxidation from proceeding through the bulk of the substrate. Other options are multilayer graphene (MLG) [62, 67], to create a spatial steric hindrance and graphene-polymer sandwiched coatings [68]. As shown in figure 7, Tiwari *et al* [67] showed that the corrosion resistance of copper has significantly improved from $1.245 \times 10^4\ \Omega\ cm^2$ (bare copper) to $6.260 \times 10^4\ \Omega\ cm^2$ after coated with MLG. Most importantly, the corrosion resistance sustained up to 386 h.

Similarly, by taking advantage of the excellent catalytic properties of nickel as substrate to grow graphene, Mills *et al* [69] has employed photothermal CVD to grow MLG sheets on nickel-plated steel (figure 8). As known, nickel is prone to oxidation which occurs instantly at the cost of the conductivity and may further induce corrosion. Figure 8(a) shows the surface of nickel oxide grains formed instantaneously due to the oxidation on nickel surface. The MLG-coated nickel-plated steel showed improved electrical properties, where its sheet resistance (R_{sh}) and interfacial contact resistance (ICR, at 140 N cm^{-2}) were found to be 2.52 $m\Omega\ sq^{-1}$ and 0.3 $m\Omega\ cm^{-2}$, respectively, counted for 10% reduction and 200 times less in comparison to those values of the pristine nickel-plated steel ($R_{sh} = 2.81\ m\Omega\ sq^{-1}$, $ICR = 61\ m\Omega\ cm^{-2}$). Impressively, it was observed that even after several years, no oxidation observed and the substrate maintains its very low R_{sh} and ICR. Thus, MLG offers excellent gas barrier, in this case inhibiting the oxidation of the outermost surface of the substrates.

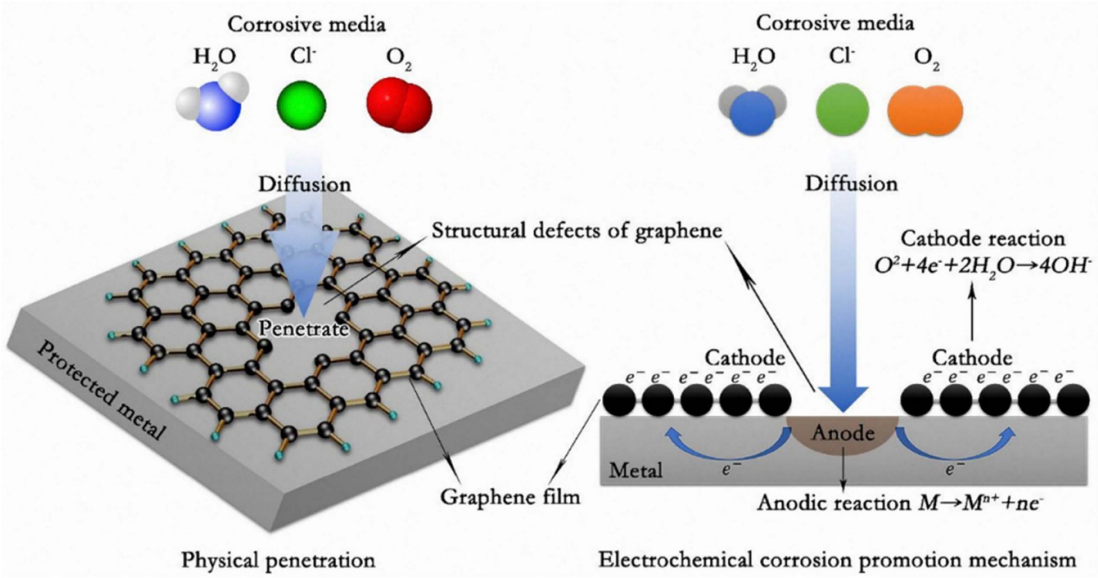

Figure 6. Galvanic cathodic corrosion promoted by defect areas in graphene. Reprinted from [64], © 2018 Elsevier B.V. All rights reserved.

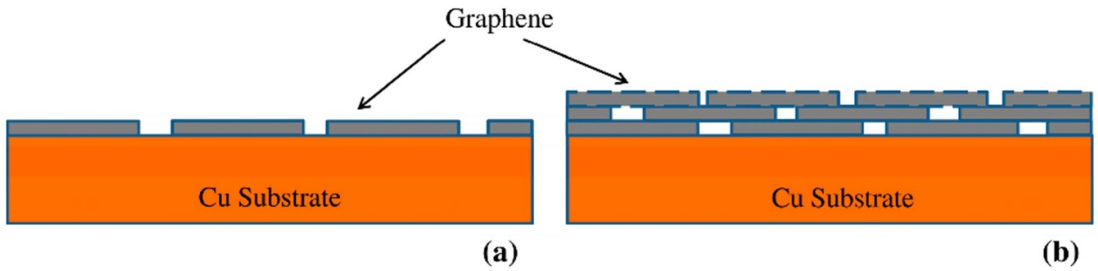

Figure 7. Schematic illustration of (a) single layer graphene where defects are exposed and (b) MLG which overlap and cover the defects. Reproduced from [67]. CC BY 4.0.

The selective passivation of graphene defects by chemical functionalization with polymeric brushes is attracting more attention now. This route is advantageous since the chemical functionalization provides high stability of the coatings but also, when the appropriate polymer and nanoparticles are chosen, the resulting composites may have synergistic effect in terms of long-term stability and durability of corrosion resistance. Therefore, the anticorrosion properties of polymeric material functionalized graphene composites will be discussed in the following section.

3.2. Anti-corrosion properties of graphene-polymer brush-composites

Several research groups have reported covalent polymer functionalization of graphene to improve corrosion properties [70–75]. Besides its excellent impermeable properties, well-dispersed graphene in polymer matrix acts as perfect physical barrier outperforms those of nano silica, zinc-oxide or titania [76]. Jin *et al* [70] reported the anticorrosion properties of poly(acrylamide-co-acrylic acid)-grafted GO (poly(AM-co-AA)-g-GO), here refers as PGMAs, on magnesium alloy substrates after immersing in 3.5% NaCl solution for 24 h (figure 9).

Figure 9(a) shows photograph images of the bare and coated samples before and after corrosion test. Using potentiodynamic polymerization curves (figure 9(b)), they found that corrosion resistance, R_{corr}, increased from 0.027 MΩ cm^2 for bare Mg alloy to 0.39 MΩ cm^2 for poly(AM-co-AA)/Mg alloy and 15.35 MΩ cm^2 for PGMAs/Mg alloy, respectively (table 1). They ascribed the enhanced corrosion protection to synergistic effects from the polymers and GO. The excellent dispersion of GO in the polymer matrix allowed GO nanosheets to fill the coating pinholes and act as physical barriers to decrease the electrolytes diffusion towards substrates. Also, polymer molecules played a bridging role in constructing compact and crosslinking structure of the coatings, which interrupt the corrosive ions and inhibit the corrosion.

Similar to the above work, Wang *et al* [71] have reported the grafting of complex poly(urethane-co-acrylates) (PUA) brushes on rGO and their enhanced corrosion protection on tin plate up to 25 d immersion in 5% NaCl solution. First, they functionalized

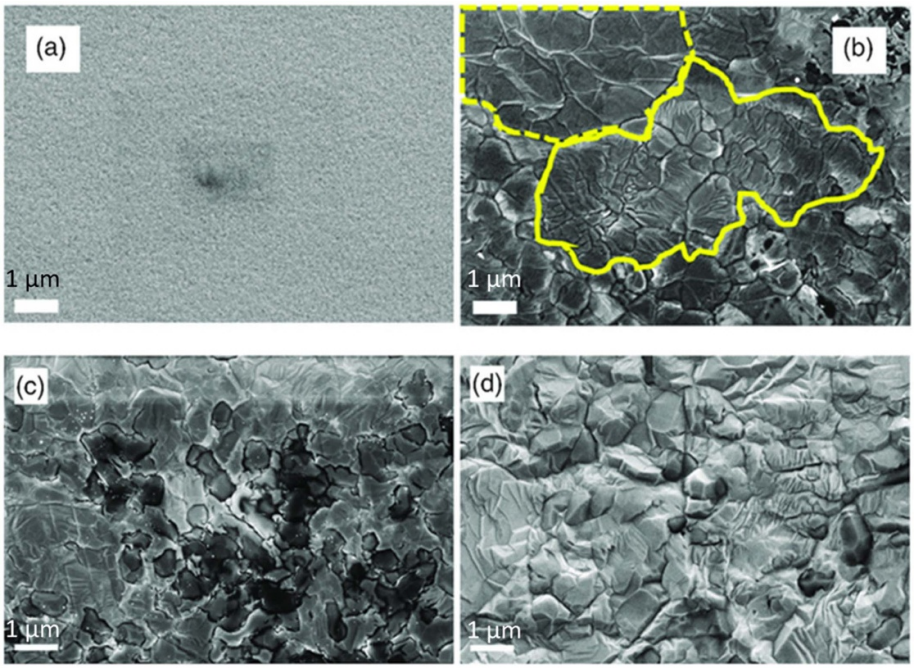

Figure 8. SEM images of (a) the pristine Ni-plated steel which is instantaneously oxidized, evidenced by the formation of nickel oxide grains. (b) MLG-coated Ni-plated steel, where clear-terracing domains (solid and dash-lines) are visible. Comparison of the MLG coating on (c) the rear and (d) the front of the substrate. Scale bar is 1 μm. Figures (a)–(d): [69] John Wiley & Sons. © 2019 WILEY-VCH Verlag GmbH & Co. KGaA, Weinheim.

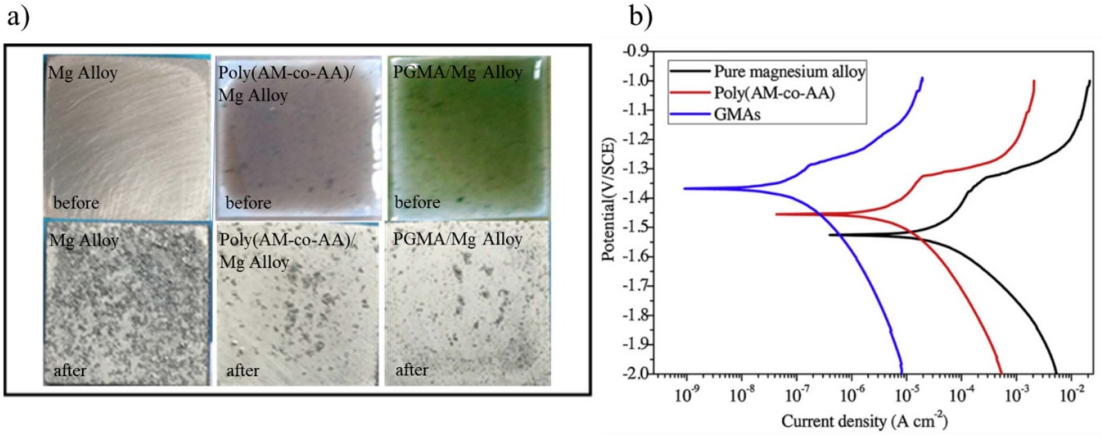

Figure 9. (a) Photograph images of bare Mg alloy, poly(AM-co-AA)/Mg alloy and PGMA/Mg alloy samples before (top) and after corrosion test (bottom). After immersion in 3.5% NaCl solution, corrosion is pronounced for uncoated Mg allow substrate while for PGMAs-coated substrate corrosion is mostly inhibited. (b) Potentiodynamic polarization curve from corrosion tests shows the PGMAs coated substrates shows the best anticorrosion performance, corroborating the optical images in (a). Figures (a) and (b): Reprinted from [70], © 2019 Elsevier B.V. All rights reserved.

GO with cetyltrimethylammonium bromide initiator followed by reduction of GO by hydrazine monohydrate to obtain functionalized cationic reduced graphene (CRG). Separately, they prepared carboxylated polyurethane which was copolymerized with acrylate monomers, namely butyl acrylate (BA), methyl methacrylate (MMA), and hydroxyl methacrylate (HEMA), to obtain waterborne PUA (WPUA) prepolymer. Subsequently, CRG was then introduced to WPUA prepolymer and APS as initiator was added to initiate radical polymerization, resulting in WPUA-CRG. They observed that compared to pristine graphene, grafting the polymers to CRG leads to the formation of well-dispersed and uniform graphene-PUA complex. They found that CRG-WPUA with 0.5% graphene content showed the best protection having the highest corrosion resistance, R_{corr}, of 18.7 MΩ cm^2 compared to 1.02 MΩ cm^2 for blank tin plate, and 2.7 MΩ cm^2 for WPUA. Increasing graphene content to 0.7% leads to a decrease of R_{corr} to 4.07 MΩ cm^2. They concluded that (a) the tortuosity of diffusion pathway of the corrosive ions is increased owing to the well-dispersibility of graphene in polymer matrix (b) the permeation of

Table 1. Potentiodynamic polarization data of the samples. Reprinted from [70], © 2019 Elsevier B.V. All rights reserved.

Samples	I_{corr} (A cm^{-2})	E_{corr} (V)	R_{corr} (MΩ cm^2)
Mg alloy	5.75×10^{-5}	−1.548	0.027
Poly(AM-co-AA)/Mg alloy	3.67×10^{-6}	−1.445	0.39
PGMAs/Mg alloy	8.84×10^{-8}	−1.357	15.35

ions through the coating becomes more difficult since the activation energy peak for the water to diffuse are increased due to the incorporated graphene within the coating, (c) direct connection between graphene–graphene and graphene–metal are inhibited by the grafted polymer. Therefore, the risk for the formation of corrosion-promoting electrode is decreased, (d) interfacial defects that lead to decrease of corrosion protection may be generated by strong phase separation of polymers and hydrophobic rGO. Therefore, the compatibility and interaction of graphene and polymer matrix are key to achieve well-dispersed and uniform graphene dispersion which play important role to increase the corrosion protection.

Recently, Zhang *et al* [72] have prepared poly(triethylene tetramine-polyethylene glycol diglycidyl ether) (TETA-DGPEG) to covalently functionalize GO. The TETA-DGPEG-functionalized GO, or TDPG, was then grafted into the WPU matrix resulting in WPU-grafted-TDPG (WPU/TDPG). They prepared composites with graphene weight ratio of 0.01%, 0.05% and 0.1% to the WPU polymer. The composites improved the corrosion protection of the Q235 steel as shown in figure 10(a).

As derived from the Tafel curve in figure 10(b), they found that the WPU/TDPG$_{0.05}$ displayed the best corrosion protection with the highest polarization protection, indicated by its shifting to the most positive value in comparison to the rest coatings, with R_p of 3.4 MΩ cm^2 (see table 2). The corrosion resistance, R_{corr}, of WPU/TPDG$_{0.05}$ increased to 23.9 MΩ cm^2 from 13.6 MΩ cm^2 for WPU. After 30 d immersion in 3.5% NaCl solution, the R_{corr} decreased to 9.5 MΩ cm^2 for WPU/TPDG$_{0.05}$ and 4.62 MΩ cm^2 for WPU, respectively.

These results corroborate with their optical assessment as shown in figure 10(a). The photograph images display that the WPU/TDPG$_{0.05}$ exhibit corrosion protection which outperform that of WPU, WPU/GO, WPU/TDPG$_{0.01}$ and WPU/TDPG$_{0.1}$. Similar to the observations by Wang *et al* [71], Zhang *et al* concluded that the covalent functionalization of graphene composites shows better corrosion protection in comparison to the non-covalent/physical blending counterparts. In agreement to these works, Wen *et al* [77] also found that polyurethane covalent grafting of GO improved corrosion protection in comparison to noncovalent grafting of GO. Thus, the covalent functionalization of graphene plays a key role to achieve well-dispersed integration of graphene into polymer matrix, where the graphene nanosheets act as physical barrier which increase the diffusion path of corrosive ions. This needs an optimal graphene loading in the polymer matrix. Higher graphene loading may cause aggregation and interfacial defects leading to decreased corrosion protection.

Among the recent works on covalent polymer functionalization on graphene to improve corrosion properties, the work by Xie *et al* [73] is impressive. They reported the preparation of polyacrylate brushes grown on GO to enhance the corrosion resistance of epoxy resins as shown in figure 11. This resulted in the anticorrosion protection of carbon steel substrates up to 40 d when immersed in 3.5% NaCl solution. They first functionalized GO with silane-based initiator and subsequently employed free radical polymerization to grow poly(glycydylmethacrylate-co-methylmethacryle) (poly(GMA-co-MMA)) brushes on GO (polyacrylate-GO (PA-GO)). In the next step, they mixed the PA-GO composites with epoxy resin to achieve epoxy/PA-GO.

The PA-GO brush-composites were well-dispersed within the epoxy matrix and were bound with the epoxy in comparison to GO. Figure 12 shows the potentiodynamic curve or Tafel plot for the samples after immersing in 3.5% NaCl for 40 d. Table 3 presents the corrosion parameters derived from Tafel plots in figure 12.

Tafel plot can be used to evaluate the quality and the corrosion properties of the coatings. Similar to the results of Zhang *et al* [72] presented in figure 10(b). It can also be seen clearly in figure 12 that the E_{corr} shifts to the more positive values, from the coating E, the coating E/GO, to the coating E/PA-GO, respectively, where the I_{corr} decreases as well. This shift clearly indicates that the coating E/PA-GO has the highest corrosion protection in comparison to the coating E and E/GO. The covalent grafting of GO with polyacrylate block copolymers (GMA and MMA) has enhanced the interface between the graphene and the polymer matrix where defects are reduced significantly and the barrier property of the graphene in the polymer matrix is increased since graphene increases the energy required to stabilize the metal ions, by preventing the anions to be formed or migrate to the location.

As can be calculated from table 3, the corrosion resistance increased to $2.29 \pm 0.15 \times 10^3$ MΩ cm^2 for epoxy/PA-GO from $7.43 \pm 0.14 \times 10^2$ MΩ cm^2 for epoxy/GO and $3.39 \pm 0.20 \times 10^{-1}$ MΩ cm^2 for pristine epoxy, respectively. Interestingly, their long-term studies showed that the epoxy/PA-GO exhibits very low corrosion rate, C_R, of

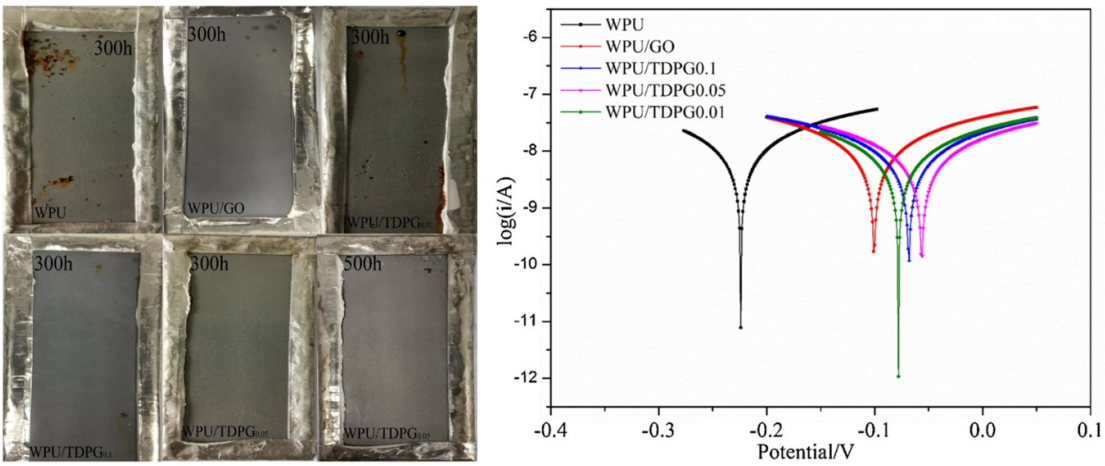

Figure 10. (a) Photograph images of the neat WPU and WPU/TDPG coated steel samples. (b) Tafel plot of different composites coatings immersed in 3.5% NaCl solutions for 10 d. WPU/TPDPG$_{0.5}$ coating sample shows the shifting to the most positive value indicates it has the highest performed barrier properties. Figures (a) and (b): Reprinted from [72], © 2020 Published by Elsevier B.V.

Table 2. Electrochemical data derived from Tafel plot in figure 10(b). Reprinted from [72], © 2020 Published by Elsevier B.V.

Samples	E_{corr} (V)	I_{corr} (A cm2)	b_a (V dec^{-1})	b_c (V dec^{-1})	R_p (MΩ cm^2)	R_{corr} (day 1) (MΩ cm^2)	R_{corr} (day 30) (MΩ cm^2)
WPU	−0.224	1.91×10^{-8}	4.94	4.96	2.30	13.6	4.62
WPU/GO	−0.101	1.74×10^{-8}	4.96	4.93	2.54	14.9	4.54
WPU/TDPG$_{0.1}$	−0.068	1.36×10^{-8}	4.91	4.97	3.25	22.3	7.69
WPU/TDPG$_{0.05}$	−0.056	1.30×10^{-8}	4.90	4.98	3.40	23.9	9.48
WPU/TDPG$_{0.01}$	−0078	1.34×10^{-8}	4.94	4.95	3.28	23.4	9.22

E_{corr}—corrosion potential; I_{corr}—corrosion current density; b_a—anodic Tafel slope; b_c—cathodic Tafel slope; R_p—polarization resistance (MΩ cm^2).

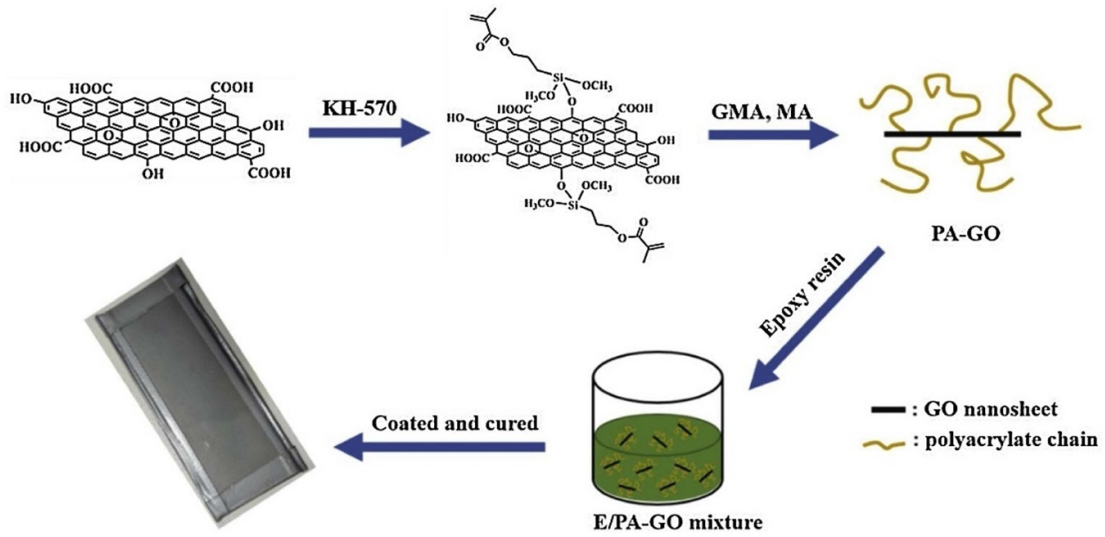

Figure 11. Schematic illustration of poly(GMA-co-MMA) brushes grown on GO and subsequently mixed with epoxy resin. Reprinted from [73], © 2020 Elsevier B.V. All rights reserved.

1.701×10^{-8} mm yr^{-1}, which is one degree of magnitude lower than that of for epoxy/GO (1.563×10^{-7} mm yr^{-1}) and for pristine epoxy, (4.814×10^{-7} mm yr^{-1}), respectively.

The anticorrosion mechanism (figure 13), is based on the mechanism reported in works discussed above [70–73]. The corrosive agents and oxygen molecules diffuse into the coating through the

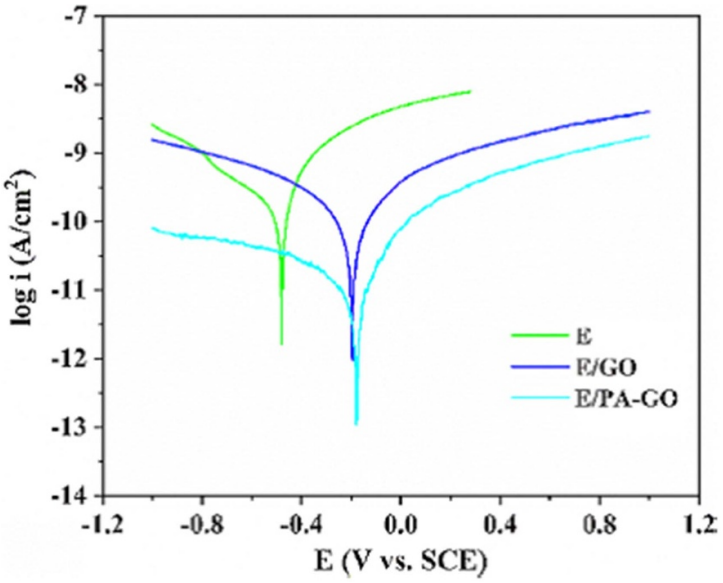

Figure 12. Tafel plot of neat epoxy (E), epoxy/GO and E/PA-GO after immersing in 3.5% NaCl for 40 d. Reprinted from [73], © 2020 Elsevier B.V. All rights reserved.

Table 3. Corrosion properties as derived from Tafel plot in figure 12. Reprinted from [73], © 2020 Elsevier B.V. All rights reserved.

Sample	E_{corr} (V)	I_{corr} (μA cm^{-2})	b_a (V dec^{-1})	b_c (V dec^{-1})	R_{corr}	C_R (mm yr^{-1})
Neat epoxy	−0.480	2.075×10^{-4}	0.167	−0.299	$3.39 \pm 0.20 \times 10^{-1}$	4.814×10^{-7}
E/GO	−0.196	6.735×10^{-5}	0.190	−0.203	$7.43 \pm 0.14 \times 10^{2}$	1.563×10^{-7}
E/PA-GO	−0.179	7.331×10^{-6}	0.140	−0.288	$2.29 \pm 0.15 \times 10^{3}$	1.701×10^{-7}

E_{corr}—corrosion potential; I_{corr}—corrosion current density; b_a—anodic Tafel slope; b_c—cathodic Tafel slope; $R_{corr} = E_{corr}/I_{corr}$—corrosion resistance; C_R—corrosion rate.

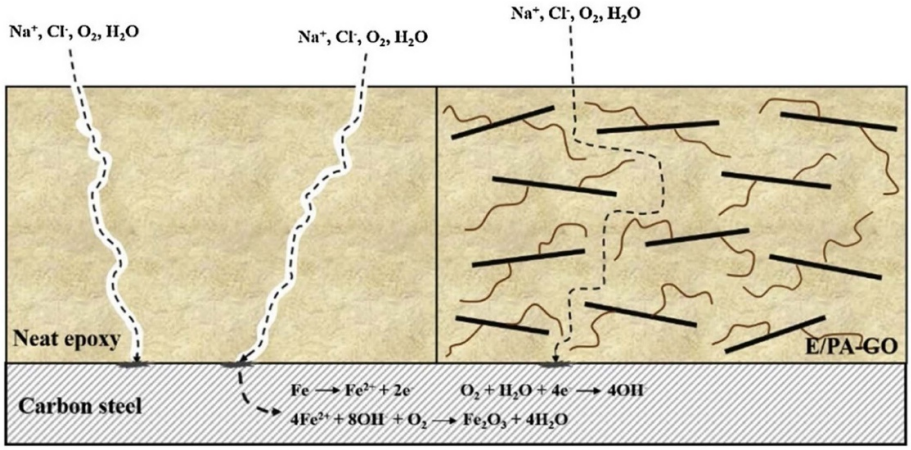

Figure 13. The mechanism of corrosion protection for epoxy/PA-GO. In comparison to neat epoxy, the epoxy/polymer-graphene composites create enhanced physical barrier that increases tortuosity pathway and delay the diffusion of anticorrosive agents. Reprinted from [73], © 2020 Elsevier B.V. All rights reserved.

defects and the micropores created by the evaporation of solvent. Hence, corrosion occurs on the interface of coating/steel when the corrosive agents reach the steel surface.

By integrating GO in epoxy, the travel path of corrosion agents and oxygen molecules increases, leading to higher time to reach the interface and slower corrosion rate. However, some defects may still be present in epoxy/GO coating due to non-optimal dispersion and binding between GO nanosheets and the epoxy matrix. Therefore, pristine GO sheets are not perfect fillers for improving epoxy coatings. On the other hand, the epoxy/PA-GO shows significantly improved anticorrosion protection. This can be

attributed to the well-dispersity of polymer brush functionalized GO nanosheets in the epoxy resin. PGMA, which is copolymer used in the epoxy/PA-GO composite, is an interesting functional polymer due to the ability of its epoxy group to react with a range of nucleophiles [78]. Obviously, the amine functional groups which are presence in the resin covalently bind with the epoxy groups [79] from the PGMA polymer resulting in a denser crosslinked polymer-epoxy matrix. Therefore, the diffusion of the corrosive agents can be disrupted by the functional groups of the polymers. In combination with the graphene materials which act as physical barrier, the epoxy/PA-GO demonstrates significantly increased anti corrosion resistance. Table 4 summarizes the above-discussed works.

4. Perspective: covalent functionalization of other 2D materials with polymeric materials and their applications as anticorrosive coatings

4.1. Hexagonal boron nitride (hBN)

The rise of graphene became a driving force for the investigation of new types of 2D materials. One of them is hBN [80, 81]. Dubbed as white-graphene, hBN exhibits remarkable optical, mechanical and thermal properties, similarly to graphene. As dielectric material with wide bandgap, hBN is chemically inert [82, 83]. Therefore, surface functionalization of hBN, both non-covalent and covalent, has become a challenging focus with more attention to the latter. One popular route, as reported by Sansburry *et al* [84] is to introduce hydroxyl functional groups to boron nitride nanosheets (BNN-OH). Cui *et al* [85] further demonstrated the covalent functionalization of BNN-OH with poly(MMA) (PMMA) resulting in composites with enhanced mechanical properties. However, to achieve BNN-OH, very strong oxidation agents are usually employed which is undesirable for large scale industrial production. Recently, Sheng *et al* [86] have extended the utilization of SIPGP to directly photograft various vinyl monomers on hBN nanosheets. Similar to graphene, the direct photografting on hBN can be realized by taking advantage of the defects present already on hBN which act as anchorage grafting site. hBN monolayer also shows anticorrosion properties [82, 83, 87]. Unlike graphene which may trigger galvanic cathodic corrosion between itself and the underlying substrates after long time exposure to the corrosive media, hBN, which is electrically insulating, poses small possibility to cause galvanic corrosion between itself and underlying substrates. With this advantage, hBN may become a competitive substitute for graphene as anticorrosion barrier coating.

In further attempt to utilize hBN as anticorrosion agent, Zhang *et al* [88] have first functionalized hBN with PDA to improve its dispersibility and then grafted γ-(2,3-epoxypropoxy) propyltrimethoxysilane (KH560). The hBN@PDA-KH560 composites showed very good dispersibility in WEC and therefore, acted as excellent anticorrosion reinforcement for WEC. The hBN@PDA-KH560/WEC showed anticorrosion protection to steel substrates immersed in 3.5% NaCl up to 25 d (R_{corr} = 30 KΩ cm^2), outperforming the neat WEC (R_{corr} = 15 K KΩ cm^2), hBN/WEC (R_{corr} = 25 KΩ cm^2) and hBN@PDA-WEC (R_{corr} = 22.5 KΩ cm^2). In a remarkable work, Wu *et al* [89] prepared partially hydroxylated hBN (BNNs) and subsequently used polyethyleneimine (PEI) to simultaneously exfoliate and functionalize the BNNs. The PEI-functionalized BNNs displayed homogenous dispersibility in waterborne epoxy (EP) coating. The PEI-BNNs/EP composites demonstrated excellent and long-term anticorrosion protection for P110 mild steel with corrosion resistance, R_{corr}, of 66.3 MΩ cm^2 after immersing in 3.5 wt% NaCl solution for 70 d, outperforming EP (R_{corr} = 0.02 MΩ cm^2), hBN/EP (R_{corr} = 0.1 MΩ cm^2) and BNNs/EP (R_{corr} = 0.15 MΩ cm^2). Despite promising, grafting of polymeric materials on hBN and its subsequent application as anticorrosion coating still gained less attention than its graphene counterpart.

4.2. $Ti_3C_2T_x$ MXene

A decade after its first discovery in 2011 [90], $Ti_3C_2T_x$ has become the most popular material in MXene family [91]. The general formula for pristine MXene is $M_{n+1}X_n$ where M is an early transition metal and X is carbon or nitrogen element. MXene is synthesized by etching selectively the A layer in the layered MAX or $M_{n+1}AX_n$ phase precursor, where A is mainly IIIA and IV elements [92, 93]. Similar to most of 2D materials, MXene shows high aspect ratio with excellent optical, electrical properties and thermal conductivity [94]. Owing to its wet chemical process, MXenes are rich in surface chemistry which make them hydrophilic and the only type of conductive 2D materials having well-dispersibility in water. Various applications of MXene such as in flexible electronics and biosensors [95], catalysis [96, 97], to energy storage [98] and electromagnetic shielding [99] have been exploited.

Despite its well-dispersibility in various solvents, grafting polymer brushes or polymer covalent functionalization on Ti_3C_2 has not yet reported. In all cases, MXene-based polymer composites are prepared by noncovalent functionalization as discussed in several recent reviews [100–104] with the exception for vanadium carbide (V_2C). Chen *et al* [105] employed SIPGP to directly photograft PDMAEMA brushes on V_2C. The stimuli-responsive behaviour of PDMAEMA allows the composite to smartly tune the transmittance and conductivity of V_2C.

Among the above-mentioned applications, Ti_3C_2-based coatings for anticorrosion is the least popular. No works on grafting of polymeric materials

Table 4. The comparison of the anticorrosion properties of graphene-based polymer composites obtained by covalent functionalization.

Graphene-polymer composites	Metal	Medium	Corrosion resistance ($M\Omega\ cm^2$)	Remark (protection)	References
Poly (AM-co-AA)-g-GO (PGMAs)	Mg alloy	3.5% NaCl solution	15.35	24 h	[70]
Poly(urethane-co-acrylates)-g-CRG Acrylates: BA, MMA, HEMA (CRG-WPUA)	Tin plate	5.0% NaCl solution	18.70	25 d	[71]
Poly(urethane-g-poly(TETA-DGPEG) ($WPU/TDPG_{0.05}$)	Steel (Q235)	3.5% NaCl solution	23.90	30 d	[72]
Epoxy/poly(GMA-co-MMA)-g-GO (Epoxy/PA-GO)	Steel	3.5% NaCl solution	2.29×10^3	40 d	[73]

on MXene, especially on Ti_3C_2, for anticorrosion protection are reported to our best knowledge. However, it is still relevant to discuss few papers found on MXene-based anticorrosion coatings. Yan *et al* [106] were among the first to demonstrate the anticorrosion properties of MXene nanosheets. They incorporated Ti_3C_2 nanosheets in epoxy resin with amine curing agent. Owing to its hydrophilic nature, Ti_3C_2 displayed well-dispersibility in the epoxy matrix, which is an important property for creating perfect physical barrier for anticorrosion agents. They prepared Ti_3C_2/epoxy composites with different loading of the Ti_3C_2 to the epoxy. Figure 14 shows the Tafel plots of the samples.

As can be seen in figure 14, the 1.0 wt% Ti_3C_2/epoxy shows the lowest I_{corr} and with the most positive E_{corr}. This indicates that the 1.0 wt% Ti_3C_2/epoxy offers the highest corrosion protection. As presented in table 5, the Ti_3C_2 clearly shows the enhancement effect for the corrosion protection of the steel substrates after 96 h immersion in 3.5% NaCl solution. The 1.0 wt% Ti_3C_2/epoxy composite gives the best protection with the highest corrosion resistance.

Similar to other work in graphene by Wen *et al* [77] higher loading of the MXene does not necessary guarantee for the best protection, rather the optimized value is necessary in order to achieve the maximum protection. Higher content of Ti_3C_2 leads to stacking of flakes creating higher volume densities. This results in phase aggregation and separation between Ti_3C_2 and the epoxy matrix, decreasing the effectiveness of $Ti_3C_2T_x$ as physical barrier for anticorrosion. Han *et al* [107] prepared Ti_3C_2/graphene (M-G) hybrid heterostructures employing PDA chemistry. The hybrid heterostructures were then incorporated within the epoxy polymer, resulting in composites with high performance for corrosion protection. Few other works on Ti_3C_2-based composites for anticorrosion have been published recently [108, 109], including Ti_3C_2/polyaniline composites [110], marking the beginning of the use of MXene for anticorrosion coating.

5. Summary and outlook

Even though graphene shows anti-corrosion properties, defects on graphene promote and accelerate corrosion. Functionalizing graphene or its derivatives such as GO with other materials improves its ability for long-term anticorrosion. For this, the common route is the non-covalent functionalization of graphene and its derivatives. However, the emerging method of covalent functionalization has advantages of long-term stability and durability. The dispersibility of graphene materials is also very important if they have to be used for commercial coatings. To improve the dispersibility, the covalent functionalization with polymer brushes is an option. An important requirement in developing the methods of functionalization is that such methods should not create any additional defects on graphene materials which may impede their anti-corrosion properties. In this review, we highlighted two methods for covalent functionalization of graphene with polymer brushes: (a) the SIPGP and (b) the PDA interfacial chemistry. These methods apparently do not create additional defects on graphene surface. Both methods are simple with no tedious steps in the synthesis process. Also, no sophisticated laboratory equipment is needed. Importantly, both methods can be easily scaled-up which is a crucial requirement for commercial application. Therefore, owing to their simplicity, these methods can be easily adopted by researchers in academia and industries working in anticorrosion field to prepare graphene-based polymer composite coatings.

Thanks to the versatility of functional polymer brushes, copolymerization and post-modification are achievable. Copolymerization can be performed by consecutive SIPGP to prepare graphene-based block copolymers for anticorrosion coatings. Post-modification such as impregnation of graphene-polymer brush composites with nanoparticles is also

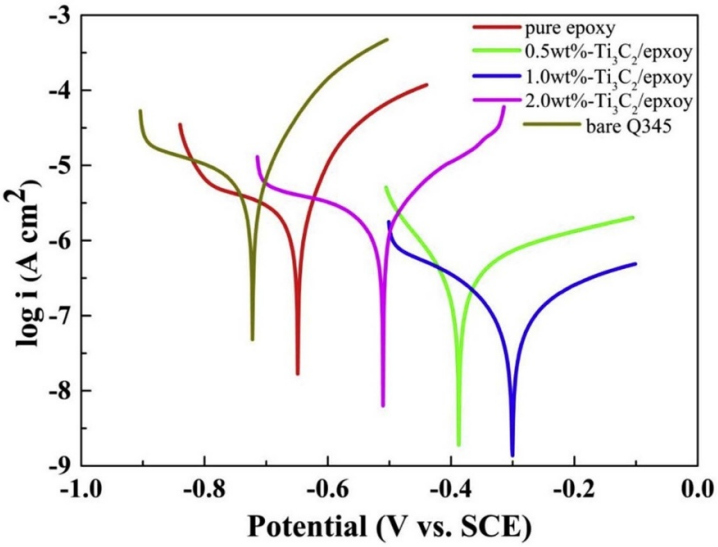

Figure 14. Tafel plots of bare Q345, pure epoxy, 0.5 wt% Ti_3C_2/epoxy, 1.0 wt% Ti_3C_2/epoxy and 2.0 wt% Ti_3C_2/epoxy coatings on Q345 steel electrodes immersed in 3.5 wt% NaCl aqueous solution for 96 h.

Table 5. The corrosion parameters for pristine and coated Q345 steel substrates after immersion for 96 h in 3.5% NaCl solution. Reprinted from [106], © 2019 Elsevier B.V. All rights reserved.

Samples	E_{corr} (V)	I_{corr} (A cm^{-2})	b_a (mV dec^{-1})	b_c (mV dec^{-1})	R_{corr} (MΩ cm^2)	C_R (mm yr^{-1})	PE (%)
Bare Q345	−0.75	7.51×10^{-5}	0.120	−0.364	0.09	87.07×10^{-3}	—
Pure epoxy	−0.71	1.00×10^{-6}	0.154	−0.369	0.71	11.62×10^{-3}	98.67%
0.5 wt% Ti_3C_2/epoxy	−0.41	1.28×10^{-7}	0.423	−0.094	3.20	1.48×10^{-3}	99.83%
1.0 wt% Ti_3C_2/epoxy	−0.29	3.39×10^{-8}	0.257	−0.218	8.55	0.39×10^{-3}	99.95%
2.0 wt% Ti_3C_2/epoxy	−0.53	7.05×10^{-7}	0.191	−0.473	0.75	8.17×10^{-3}	99.06%

E_{corr}—corrosion potential; I_{corr}—corrosion current density; b_a—anodic Tafel slope; b_c—cathodic Tafel slope; R_{corr}—corrosion resistance; C_R—corrosion rate; PE—protection efficiency.

easily realizable. However, the combination of covalent polymer-functionalized graphene nanoparticles or metal oxide nanoparticles for anticorrosion is not studied yet. Such composites are expected to show synergistic effects leading to enhanced anticorrosion properties. Also, other additional functionalities such as self-healing properties to repair defects can be expected when the right materials or polymer brushes are chosen for covalent functionalization. Examples are PDA, PDMAEMA, PGMA, and the utilization of metal oxide nanoparticles such as ZnO, CeO_2 or ZrO_2. These materials, like graphene, also exhibit impermeability or anticorrosion properties. The synergistic impermeability of these composite materials may result in excellent barriers preventing the diffusion of the corrosive media into the coating. Therefore, superior anticorrosion properties, long-term stability and durability can be achieved.

Recent results show that the covalent functionalization of graphene with polymers leads to superior corrosion protection in comparison to its non-covalent counterparts. The improvements can be attributed to (a) the increase of the diffusion pathway of the corrosive agents in reaching the substrates because graphene nanosheets which are well-dispersed in the polymer matrix act as perfect physical barrier (b) the permeation of ions through the coating becomes more difficult since the activation energy peak for the water diffusion increase by the addition of graphene (c) direct contact between graphene–graphene and graphene–metal is inhibited by the polymers grafted on graphene. This inhibition decreases the risk for the formation of corrosion-promoting electrode. Higher graphene loading not necessarily leads to increase of corrosion performance. When the loading is too high, (d) graphene and its derivatives may agglomerate, triggering a strong phase separation between polymers and graphene. As a result, interfacial defects are generated, decreasing the corrosion resistance, (e) the compact structure and crosslinking framework within the coating constructed by the polymer molecules will interrupt

the corrosive ions and inhibit the corrosion. Therefore, the compatibility and interaction of graphene-based materials and polymer matrix plays an important role in achieving well-dispersed graphene that is homogenously distributed within a compact defect-free structure, which is the key in enhancing the corrosion protection.

The strategy of covalent functionalization of graphene with polymeric materials can also be adopted to prepare composites of other 2D materials and polymers which may broaden the materials of choices for anticorrosion coatings. As an example, hBN-based polymer composites also exhibit superior anticorrosion properties. However, this possibility is still overlooked, probably due to the challenges in functionalizing hBN, which can be overcome by using the methods we have presented here. Ti_3C_2, the rising star of MXene family, is also promising as an anticorrosion barrier owing to its hydrophilic nature and well-dispersibility in water and other polar solvents. Grafting polymers on Ti_3C_2 is easier than on graphene or hBN. Surprisingly, we could not find any report on the grafting of polymers on Ti_3C_2 and the application of resulting composites as anticorrosion coating. Therefore, the use of Ti_3C_2 or MXenes in general in anticorrosion coatings still needs to be explored.

The research in anticorrosion coatings is a multidisciplinary task, rather than simple one. The involvement of researchers from chemistry, especially polymer chemistry, physics, engineering and electrochemistry will guarantee the success of the research, starting from harvesting the idea to the experimental design and the realization of the coatings with the best anticorrosion performance.

Data availability statement

No new data were created or analysed in this study.

Acknowledgments

I A and N R S thank the Dutch Research Council (De Nederlandse Organisatie voor Wetenschappelijk Onderzoek; NWO) for a LIFT Grant (731.017.413).

ORCID iD

N Raveendran Shiju https://orcid.org/0000-0001-7943-5864

References

[1] Hou B *et al* 2017 The cost of corrosion in China *npj Mater. Degrad.* **1** 4
[2] Gharbi O *et al* 2018 Chromate replacement: what does the future hold? *npj Mater. Degrad.* **2** 12
[3] Kendig M W and Buchheit R G 2003 Corrosion Inhibition of aluminum and aluminum alloys by soluble chromates, chromate coatings, and chromate-free coatings *Corrosion* **59** 379–400
[4] Kimbrough D E *et al* 1999 A critical assessment of chromium in the environment *Crit. Rev. Environ. Sci. Technol.* **29** 1–46
[5] Salnikow K and Zhitkovich A 2008 Genetic and epigenetic mechanisms in metal carcinogenesis and cocarcinogenesis: nickel, arsenic, and chromium *Chem. Res. Toxicol.* **21** 28–44
[6] Chen S *et al* 2011 Oxidation resistance of graphene-coated Cu and Cu/Ni alloy *ACS Nano* **5** 1321–7
[7] Prasai D *et al* 2012 Graphene: corrosion-inhibiting coating *ACS Nano* **6** 1102–8
[8] Geim A K and Novoselov K S 2007 The rise of graphene *Nat. Mater.* **6** 183–91
[9] Nair R R *et al* 2008 Fine structure constant defines visual transparency of graphene *Science* **320** 1308
[10] Castro Neto A H *et al* 2009 The electronic properties of graphene *Rev. Mod. Phys.* **81** 109–62
[11] Papageorgiou D G *et al* 2020 Mechanisms of mechanical reinforcement by graphene and carbon nanotubes in polymer nanocomposites *Nanoscale* **12** 2228–67
[12] Fan F R and Wu W 2019 Emerging devices based on two-dimensional monolayer materials for energy harvesting *Research* **2019** 7367828
[13] Guo C X, Guai G H and Li C M 2011 Graphene based materials: enhancing solar energy harvesting *Adv. Energy Mater.* **1** 448–52
[14] Zhu J *et al* 2014 Graphene and graphene-based materials for energy storage applications *Small* **10** 3480–98
[15] Shao Y *et al* 2015 Graphene-based materials for flexible supercapacitors *Chem. Soc. Rev.* **44** 3639–65
[16] Machado B F and Serp P 2012 Graphene-based materials for catalysis *Catal. Sci. Technol.* **2** 54–75
[17] Zhang L-H *et al* 2020 Nanocarbon catalysts: recent understanding regarding the active sites *Adv. Sci.* **7** 1902126
[18] Gitis V, Chung S-H and Raveendran Shiju N 2018 Conversion of furfuryl alcohol into butyl levulinate with graphite oxide and reduced graphite oxide *FlatChem* **10** 39–44
[19] Justino C I L *et al* 2017 Graphene based sensors and biosensors *TrAC Trends Anal. Chem.* **91** 53–66
[20] Bhardwaj S K *et al* 2019 Bi-enzyme functionalized electro-chemically reduced transparent graphene oxide platform for triglyceride detection *Biomater. Sci.* **7** 1598–606
[21] Bolotsky A *et al* 2019 Two-dimensional materials in biosensing and healthcare: from *in vitro* diagnostics to optogenetics and beyond *ACS Nano* **13** 9781–810
[22] Rodriguez R D *et al* 2020 Beyond graphene oxide: laser engineering functionalized graphene for flexible electronics *Mater. Horiz.* **7** 1030–41
[23] Bunch J S *et al* 2008 Impermeable atomic membranes from graphene sheets *Nano Lett.* **8** 2458–62
[24] Georgakilas V *et al* 2012 Functionalization of graphene: covalent and non-covalent approaches, derivatives and applications *Chem. Rev.* **112** 6156–214
[25] Criado A *et al* 2015 The covalent functionalization of graphene on substrates *Angew. Chem., Int. Ed.* **54** 10734–50
[26] Chen T, Amin I and Jordan R 2012 Patterned polymer brushes *Chem. Soc. Rev.* **41** 3280–96
[27] Chen W-L *et al* 2017 50th anniversary perspective: polymer brushes: novel surfaces for future materials *Macromolecules* **50** 4089–113
[28] Stuart M A C *et al* 2010 Emerging applications of stimuli-responsive polymer materials *Nat. Mater.* **9** 101–13
[29] Krishnamoorthy M *et al* 2014 Surface-initiated polymer brushes in the biomedical field: applications in membrane science, biosensing, cell culture, regenerative medicine and antibacterial coatings *Chem. Rev.* **114** 10976–1026
[30] Mocny P and Klok H-A 2020 Complex polymer topologies and polymer—nanoparticle hybrid films prepared via surface-initiated controlled radical polymerization *Prog. Polym. Sci.* **100** 101185

[31] Croll S G 2020 Surface roughness profile and its effect on coating adhesion and corrosion protection: a review *Prog. Org. Coat.* **148** 105847
[32] Cui G *et al* 2020 A comprehensive review on smart anti-corrosive coatings *Prog. Org. Coat.* **148** 105821
[33] Cui G *et al* 2019 A comprehensive review on graphene-based anti-corrosive coatings *Chem. Eng. J.* **373** 104–21
[34] Huang H *et al* 2020 Two-dimensional nanomaterials for anticorrosive polymeric coatings: a review *Ind. Eng. Chem. Res.* **59** 15424–46
[35] Othman N H *et al* 2019 Graphene-based polymer nanocomposites as barrier coatings for corrosion protection *Prog. Org. Coat.* **135** 82–99
[36] Englert J M *et al* 2011 Covalent bulk functionalization of graphene *Nat. Chem.* **3** 279–86
[37] Park J and Yan M 2013 Covalent functionalization of graphene with reactive intermediates *Acc. Chem. Res.* **46** 181–9
[38] Hafner D *et al* 2016 Mussel-inspired polymer carpets: direct photografting of polymer brushes on polydopamine nanosheets for controlled cell adhesion *Adv. Mater.* **28** 1489–94
[39] Sheng W *et al* 2020 Polymer brushes on graphitic carbon nitride for patterning and as a SERS active sensing layer via incorporated nanoparticles *ACS Appl. Mater. Interfaces* **12** 9797–805
[40] Amin I *et al* 2010 Polymer carpets *Small* **6** 1623–30
[41] Wright A N 1967 Surface photopolymerization of vinyl and diene monomers *Nature* **215** 953–5
[42] Steenackers M *et al* 2011 Polymer brushes on graphene *J. Am. Chem. Soc.* **133** 10490–8
[43] Seifert M *et al* 2013 Functional polymer brushes on hydrogenated graphene *Chem. Mater.* **25** 466–70
[44] Zhang T *et al* 2018 Bottom-up fabrication of graphene-based conductive polymer carpets for optoelectronics *J. Mater. Chem.* C **6** 4919–27
[45] Deshpande P P *et al* 2014 Conducting polymers for corrosion protection: a review *J. Coat. Technol. Res.* **11** 473–94
[46] Spinks G M *et al* 2002 Electroactive conducting polymers for corrosion control *J. Solid State Electrochem.* **6** 85–100
[47] Sheng X *et al* 2016 Synthesis of functionalized graphene/polyaniline nanocomposites with effective synergistic reinforcement on anticorrosion *Ind. Eng. Chem. Res.* **55** 8576–85
[48] Matyjaszewski K 2012 Atom transfer radical polymerization (ATRP): current status and future perspectives *Macromolecules* **45** 4015–39
[49] Lee H *et al* 2007 Mussel-inspired surface chemistry for multifunctional coatings *Science* **318** 426–30
[50] Hafner D and Jordan R 2020 Substrate-independent Cu(0)-mediated controlled radical polymerization: grafting of block copolymer brushes from poly(dopamine) modified surfaces *Polym. Chem.* **11** 2129–36
[51] Liu Y, Ai K and Lu L 2014 Polydopamine and its derivative materials: synthesis and promising applications in energy, environmental, and biomedical fields *Chem. Rev.* **114** 5057–115
[52] Ye Q, Zhou F and Liu W 2011 Bioinspired catecholic chemistry for surface modification *Chem. Soc. Rev.* **40** 4244–58
[53] Kang S M *et al* 2011 Simultaneous reduction and surface functionalization of graphene oxide by mussel-inspired chemistry *Adv. Funct. Mater.* **21** 108–12
[54] Luo J *et al* 2016 Mussel inspired preparation of polymer grafted graphene as a bridge between covalent and noncovalent methods *Chem. Eng. J.* **293** 171–81
[55] Wang S *et al* 2019 Polymer brushes grafted from graphene via bioinspired polydopamine chemistry and activators regenerated by electron transfer atom transfer radical polymerization *J. Polym. Sci.* A **57** 689–98
[56] Zhang B *et al* 2019 Enhanced antifouling and anticorrosion properties of stainless steel by biomimetic anchoring PEGDMA-cross-linking polycationic brushes *Ind. Eng. Chem. Res.* **58** 7107–19
[57] Cui M *et al* 2018 Polydopamine coated graphene oxide for anticorrosive reinforcement of water-borne epoxy coating *Chem. Eng. J.* **335** 255–66
[58] Qian B *et al* 2019 Mussel-inspired self-healing coatings based on polydopamine-coated nanocontainers for corrosion protection *ACS Appl. Mater. Interfaces* **11** 10283–91
[59] Chen C *et al* 2020 Bio-inspired superior barrier self-healing coating: self-assemble of graphene oxide and polydopamine-coated halloysite nanotubes for enhancing corrosion resistance of waterborne epoxy coating *Prog. Org. Coat.* **139** 105402
[60] Zhu M *et al* 2016 Low-temperature *in situ* growth of graphene on metallic substrates and its application in anticorrosion *ACS Appl. Mater. Interfaces* **8** 502–10
[61] Zhang T *et al* 2018 Polymerization driven monomer passage through monolayer chemical vapour deposition graphene *Nat. Commun.* **9** 4051
[62] Schriver M *et al* 2013 Graphene as a long-term metal oxidation barrier: worse than nothing *ACS Nano* **7** 5763–8
[63] Hsieh Y-P *et al* 2014 Complete corrosion inhibition through graphene defect passivation *ACS Nano* **8** 443–8
[64] Ding R *et al* 2018 A brief review of corrosion protective films and coatings based on graphene and graphene oxide *J. Alloys Compd.* **764** 1039–55
[65] Lee J and Berman D 2018 Inhibitor or promoter: insights on the corrosion evolution in a graphene protected surface *Carbon* **126** 225–31
[66] Weatherup R S *et al* 2015 Long-term passivation of strongly interacting metals with single-layer graphene *J. Am. Chem. Soc.* **137** 14358–66
[67] Tiwari A and Singh Raman R K 2017 Durable corrosion resistance of copper due to multi-layer graphene *Materials* **10** 1112
[68] Yu F *et al* 2018 Complete long-term corrosion protection with chemical vapor deposited graphene *Carbon* **132** 78–84
[69] Mills C A *et al* 2019 Improvement in the electrical properties of nickel-plated steel using graphitic carbon coatings *Adv. Eng. Mater.* **21** 1900408
[70] Jin T *et al* 2019 Corrosion resistance of copolymerization of acrylamide and acrylic acid grafted graphene oxide composite coating on magnesium alloy *Prog. Org. Coat.* **136** 105222
[71] Wang H *et al* 2018 A waterborne uniform graphene-poly(urethane-acrylate) complex with enhanced anticorrosive properties enabled by ionic interaction *Chem. Eng. J.* **351** 939–51
[72] Zhang F *et al* 2020 The effect of functional graphene oxide nanoparticles on corrosion resistance of waterborne polyurethane *Colloids Surf.* A **591** 124565
[73] Xie Y *et al* 2020 A novel approach to fabricate polyacrylate modified graphene oxide for improving the corrosion resistance of epoxy coatings *Colloids Surf.* A **593** 124627
[74] Mohammadkhani R *et al* 2020 Designing a dual-functional epoxy composite system with self-healing/barrier anti-corrosion performance using graphene oxide nano-scale platforms decorated with zinc doped-conductive polypyrrole nanoparticles with great environmental stability and non-toxicity *Chem. Eng. J.* **382** 122819
[75] Rajitha K and Mohana K N 2020 Application of modified graphene oxide—polycaprolactone nanocomposite coating for corrosion control of mild steel in saline medium *Mater. Chem. Phys.* **241** 122050
[76] Peng T *et al* 2020 Polymer nanocomposite-based coatings for corrosion protection *Chem.—Asian J.* **15** 3915–41
[77] Wen J-G *et al* 2019 Improvement of corrosion resistance of waterborne polyurethane coatings by covalent and

noncovalent grafted graphene oxide nanosheets *ACS Omega* **4** 20265–74
[78] Gauthier M A, Gibson M I and Klok H-A 2009 Synthesis of functional polymers by post-polymerization modification *Angew. Chem., Int. Ed.* **48** 48–58
[79] Majer J *et al* 2019 *In situ* hyper-cross-linking of glycidyl methacrylate–based polyHIPEs through the amine-enriched high internal phase emulsions *Colloid Polym. Sci.* **297** 239–47
[80] Weng Q *et al* 2016 Functionalized hexagonal boron nitride nanomaterials: emerging properties and applications *Chem. Soc. Rev.* **45** 3989–4012
[81] Lin Y and Connell J W 2012 Advances in 2D boron nitride nanostructures: nanosheets, nanoribbons, nanomeshes and hybrids with graphene *Nanoscale* **4** 6908–39
[82] Li L H *et al* 2014 Strong oxidation resistance of atomically thin boron nitride nanosheets *ACS Nano* **8** 1457–62
[83] Liu Z *et al* 2013 Ultrathin high-temperature oxidation-resistant coatings of hexagonal boron nitride *Nat. Commun.* **4** 2541
[84] Sainsbury T *et al* 2012 Oxygen radical functionalization of boron nitride nanosheets *J. Am. Chem. Soc.* **134** 18758–71
[85] Cui Z, Martinez A P and Adamson D H 2015 PMMA functionalized boron nitride sheets as nanofillers *Nanoscale* **7** 10193–7
[86] Sheng W *et al* 2019 Polymer brushes on hexagonal boron nitride *Small* **15** 1805228
[87] Mahvash F *et al* 2017 Corrosion resistance of monolayer hexagonal boron nitride on copper *Sci. Rep.* **7** 42139
[88] Zhang C *et al* 2017 Poly(dopamine) assisted epoxy functionalization of hexagonal boron nitride for enhancement of epoxy resin anticorrosion performance *Polym. Adv. Technol.* **28** 214–21
[89] Wu Y *et al* 2020 Synergistic functionalization of h-BN by mechanical exfoliation and PEI chemical modification for enhancing the corrosion resistance of waterborne epoxy coating *Prog. Org. Coat.* **142** 105541
[90] Naguib M *et al* 2011 Two-dimensional nanocrystals produced by exfoliation of Ti_3AlC_2 *Adv. Mater.* **23** 4248–53
[91] Fu Z *et al* 2019 Rational design of flexible two-dimensional MXenes with multiple functionalities *Chem. Rev.* **119** 11980–2031
[92] Ng W H K *et al* 2018 The Ti_3AlC_2 MAX phase as an efficient catalyst for oxidative dehydrogenation of n-butane *Angew. Chem., Int. Ed.* **57** 1485–90
[93] Ronda-Lloret M *et al* 2020 Butane dry reforming catalyzed by cobalt oxide supported on Ti_2AlC MAX phase *ChemSusChem* **13** 6401–8
[94] Jiang X *et al* 2020 Two-dimensional MXenes: from morphological to optical, electric, and magnetic properties and applications *Phys. Rep.* **848** 1–58
[95] Huang W *et al* 2020 Recent advances in functional 2D MXene-based nanostructures for next-generation devices *Adv. Funct. Mater.* **30** 2005223
[96] Slot T K *et al* 2021 Enhancing catalytic epoxide ring-opening selectivity using surface-modified $Ti_3C_2T_x$ MXenes *2D Mater.* **8** 035003
[97] Slot T K *et al* 2020 Surface oxidation of $Ti_3C_2T_x$ enhances the catalytic activity of supported platinum nanoparticles in ammonia borane hydrolysis *2D Mater.* **8** 015001
[98] Xu X *et al* 2021 Progress and perspective: MXene and MXene-based nanomaterials for high-performance energy storage devices *Adv. Electron. Mater.* **7** 2000967
[99] Han M *et al* 2020 Beyond $Ti_3C_2T_x$: MXenes for electromagnetic interference shielding *ACS Nano* **14** 5008–16
[100] Carey M and Barsoum M W 2021 MXene polymer nanocomposites: a review *Mater. Today Adv.* **9** 100120
[101] Gao L *et al* 2020 MXene/polymer membranes: synthesis, properties, and emerging applications *Chem. Mater.* **32** 1703–47
[102] Jimmy J and Kandasubramanian B 2020 Mxene functionalized polymer composites: synthesis and applications *Eur. Polym. J.* **122** 109367
[103] Chen X *et al* 2021 MXene/polymer nanocomposites: preparation, properties, and applications *Polym. Rev.* **61** 80–115
[104] Riazi H *et al* 2021 Ti_3C_2 MXene–polymer nanocomposites and their applications *J. Mater. Chem.* A **9** 8051–98
[105] Chen J *et al* 2015 CO_2 and temperature dual responsive 'smart' MXene phases *Chem. Commun.* **51** 314–7
[106] Yan H *et al* 2019 Ti_3C_2 MXene nanosheets toward high-performance corrosion inhibitor for epoxy coating *Prog. Org. Coat.* **135** 156–67
[107] Yan H *et al* 2020 Towards high-performance additive of Ti_3C_2/graphene hybrid with a novel wrapping structure in epoxy coating *Carbon* **157** 217–33
[108] Sheng X *et al* 2021 Anticorrosive and UV-blocking waterborne polyurethane composite coating containing novel two-dimensional Ti_3C_2 MXene nanosheets *J. Mater. Sci.* **56** 4212–24
[109] Zhao H *et al* 2021 Air-stable titanium carbide MXene nanosheets for corrosion protection *ACS Appl. Nano Mater.* **4** 3075–86
[110] Cai M *et al* 2021 $Ti_3C_2T_x$/PANI composites with tunable conductivity towards anticorrosion applicatio*n Chem. Eng. J.* **410** 128310